Loss-of-Function Mutations in *WDR73* Are Responsible for Microcephaly and Steroid-Resistant Nephrotic Syndrome: Galloway-Mowat Syndrome

Estelle Colin,[1,2,15] Evelyne Huynh Cong,[3,4,15] Géraldine Mollet,[3,4] Agnès Guichet,[1] Olivier Gribouval,[3,4] Christelle Arrondel,[3,4] Olivia Boyer,[3,4,5] Laurent Daniel,[6] Marie-Claire Gubler,[3,4,5] Zelal Ekinci,[7] Michel Tsimaratos,[8] Brigitte Chabrol,[9] Nathalie Boddaert,[4,10] Alain Verloes,[11] Arnaud Chevrollier,[1,2] Naig Gueguen,[1,2] Valérie Desquiret-Dumas,[1,2] Marc Ferré,[1,2] Vincent Procaccio,[1,2] Laurence Richard,[12] Benoit Funalot,[12] Anne Moncla,[13] Dominique Bonneau,[1,2,16] and Corinne Antignac[3,4,14,16,*]

Galloway-Mowat syndrome is a rare autosomal-recessive condition characterized by nephrotic syndrome associated with microcephaly and neurological impairment. Through a combination of autozygosity mapping and whole-exome sequencing, we identified *WDR73* as a gene in which mutations cause Galloway-Mowat syndrome in two unrelated families. *WDR73* encodes a WD40-repeat-containing protein of unknown function. Here, we show that WDR73 was present in the brain and kidney and was located diffusely in the cytoplasm during interphase but relocalized to spindle poles and astral microtubules during mitosis. Fibroblasts from one affected child and WDR73-depleted podocytes displayed abnormal nuclear morphology, low cell viability, and alterations of the microtubule network. These data suggest that WDR73 plays a crucial role in the maintenance of cell architecture and cell survival. Altogether, *WDR73* mutations cause Galloway-Mowat syndrome in a particular subset of individuals presenting with late-onset nephrotic syndrome, postnatal microcephaly, severe intellectual disability, and homogenous brain MRI features. *WDR73* is another example of a gene involved in a disease affecting both the kidney glomerulus and the CNS.

Introduction

Galloway-Mowat syndrome (GMS [MIM 251300]) is a rare autosomal-recessive disorder characterized by the combination of nephrotic syndrome (NS) and various CNS abnormalities.[1] Since the first report by Galloway and Mowat in 1968,[2] more than 60 cases of GMS have been reported.[3] Several case reports and studies on small series describing the clinical and histopathological features of GMS have revealed the clinical heterogeneity of this condition. Although some authors have tried to categorize GMS according to clinical presentation,[4] no classification is currently accepted for this disease. The consistent morphological hallmark is microcephaly, which is often present at birth (primary microcephaly) but might also develop postnatally (secondary microcephaly). Major brain abnormalities include cerebral atrophy and neural-migration defects, such as agyria, microgyria, or polymicrogyria. These structural brain abnormalities are associated with severe psychomotor impairment, hypotonia, and seizures in half of all cases. Renal manifestations of GMS range from isolated proteinuria to overt, steroid-resistant NS, which rapidly progresses to end-stage kidney disease (ESKD) after a few months. Although NS is typically detected in the first months of life, later onset during childhood (44–198 months) has been reported in a few cases.[5–7] The anatomopathological lesions observed in kidney biopsies include minimal changes, focal segmental glomerulosclerosis (FSGS) that might be of the collapsing type, and diffuse mesangial sclerosis, which is sometimes difficult to distinguish from FSGS.[8] The prognosis of GMS is poor, and most affected children die before the age of 6 years.

Although a growing number of genes have been implicated in syndromic and nonsyndromic hereditary NS, the molecular basis of GMS is currently unknown. Given its clinical heterogeneity, it is likely that this syndrome is genetically heterogeneous. In a previous study,[9] an analysis of candidate genes encoding proteins of the glomerular basement membrane (*LAMB2* [MIM 150325] and *LAMA5* [MIM 601033]) or podocyte proteins (*ITGB1*

[1]Department of Biochemistry and Genetics, Angers University Hospital, 49933 Angers, France; [2]Centre National de la Recherche Scientifique 6214 and Institut National de la Santé et de la Recherche Médicale 1083, Université Nantes Angers Le Mans, 49000 Angers, France; [3]Institut National de la Santé et de la Recherche Médicale Unité Mixte de Recherche 1163, Laboratory of Inherited Kidney Diseases, 75015 Paris, France; [4]Université Paris Descartes, Sorbonne Paris Cité, Imagine Institute, 75015 Paris, France; [5]Department of Pediatric Nephrology, Necker Hospital, Assistance Publique – Hôpitaux de Paris, 75015 Paris, France; [6]Department of Pathology, Timone Hospital, Assistance Publique – Hôpitaux de Marseille, 13385 Marseille, France; [7]Department of Pediatric Nephrology, Faculty of Medicine, Kocaeli University, 41380 Kocaeli, Turkey; [8]Department of Pediatric Nephrology, Timone Hospital, Assistance Publique – Hôpitaux de Marseille, 13385 Marseille, France; [9]Department of Pediatric Neurology, Timone Hospital, Assistance Publique – Hôpitaux de Marseille, 13385 Marseille, France; [10]Department of Pediatric Radiology, Necker Hospital, Assistance Publique – Hôpitaux de Paris, 75015 Paris, France; [11]Department of Genetics, Robert Debré Hospital, Assistance Publique – Hôpitaux de Paris and Université Paris Diderot, 75015 Paris, France; [12]Departments of Neurology, Biochemistry, and Genetics, Limoges University Hospital, 87000 Limoges, France; [13]Department of Genetics, Timone Hospital, Assistance Publique – Hôpitaux de Marseille, 13385 Marseille, France; [14]Department of Genetics, Necker Hospital, Assistance Publique – Hôpitaux de Paris, 75015 Paris, France
[15]These authors contributed equally to this work
[16]These authors contributed equally to this work
*Correspondence: corinne.antignac@inserm.fr
http://dx.doi.org/10.1016/j.ajhg.2014.10.011.

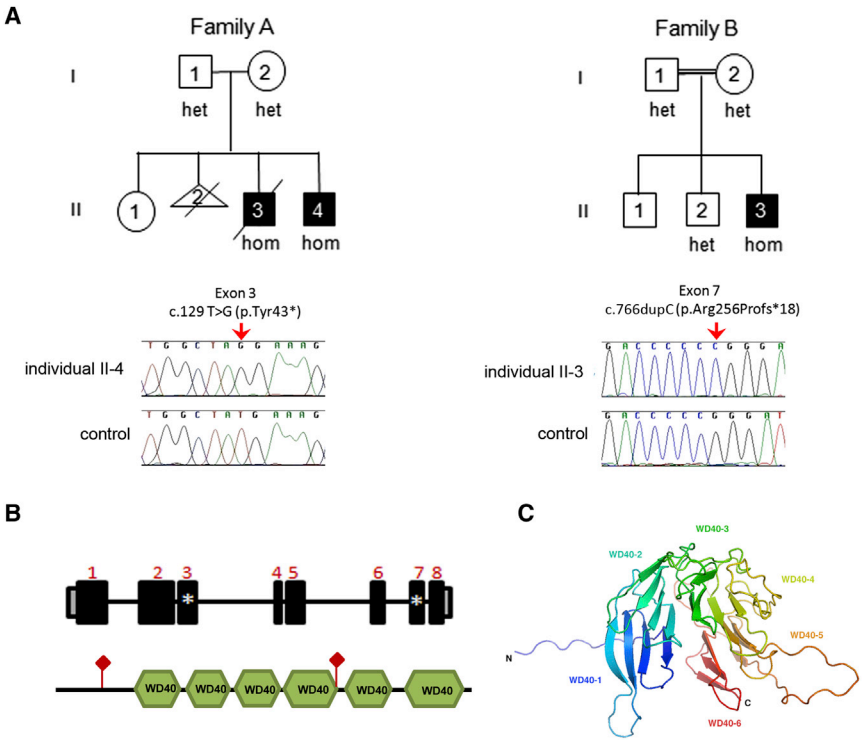

Figure 1. Identification of *WDR73* Mutations, Gene Structure, and Protein Structure

(A) Pedigrees of families A and B. The affected status is indicated by filled symbols, and the allele status is given below each tested individual. Representative chromatograms show the homozygous c.129 T>G (p.Tyr43*) and c.766dupC (p.Arg256Profs*18) mutations and the wild-type allele. Red arrows indicate the position of the nucleotide changes. Abbreviations are as follows: het, heterozygous; and hom, homozygous.

(B) Schematic overview of the eight exons (black boxes) of human *WDR73* and of the six WD40 repeats (green hexagons) predicted in WDR73. Asterisks (for the gene) and red diamonds (for the protein) denote the two mutations described in this article.

(C) Model of residues 73–370 of human WDR73 (GenBank AAF28942.1). WDR73 is shown as a rainbow-spectrum cartoon showing the six-bladed β sheets. Blades are numbered 1–6, and the direction of the polypeptide chain is indicated by a color ramp (N-terminal in blue and C-terminal in red) along the length of the ribbon.

[MIM 135630], *ITGA3* [MIM 605025], and *ACTN4* [MIM 604638]) failed to detect any causative mutation in a cohort of 18 GMS-affected individuals.

In this study, we used whole exome sequencing (WES) to identify *WDR73* mutations in two families affected by GMS. We demonstrated that the localization of the *WDR73* product, a WD40-repeat-containing protein, was cell-cycle dependent. WDR73 was diffuse in the cytosol during interphase and enriched at the spindle poles and microtubule asters during mitosis. Functional studies in fibroblasts from one affected child and in WDR73-depleted podocytes revealed that loss of WDR73 led to defects in cell survival and microtubule organization, and these might explain the dual neurologic and renal phenotype in this subset of individuals with GMS.

Subjects and Methods

Human Studies

Genomic DNA was isolated from blood or from cultured skin fibroblasts by standard procedures. Written informed consent was obtained from each subject involved in this study or from parents of subjects under 18 years of age. The study protocol was approved by two institutional review boards (Comité de Protection des Personnes Ile de France II and Comité d'Éthique du Centre Hospitalier Universitaire d'Angers) in accordance with French law. Pedigrees of the families involved in this study are shown in Figure 1A.

Autozygosity Mapping and WES

Although no consanguinity was known in family A, we hypothesized that the parents could be related because of their close geographical origins. We performed a genome-wide search with SNP microarrays (Illumina Human 660W-Quad ADN v.1.C) to identify shared runs of homozygosity (ROHs) in the two affected children (II-3 and II-4, both from family A). Data were interpreted with Illumina GenomeStudio v.2010.3 and CNVPartition v.3.1.6 (Illumina Genotyping v.1.8.4 Genome Viewer v.1.8). Analyses were mapped to the human reference genome sequence (UCSC Genome Browser assembly GRCh37/hg19).

WES was performed in individual II-3 from family A (Figure 1A) at Integragen (Evry). Whole-exome capture was performed with the SureSelect Human All Exon Kit v.2 (Agilent Technologies). The enriched library was then sequenced on an Illumina HiSeq 2000 (2 × 75 bases). Images were analyzed and the bases were determined with the pipeline Illumina RTA v.1.14 (CASAVA 1.8). Reads were mapped to the human reference genome sequence (UCSC Genome Browser assembly GRCh37/hg19). We subsequently applied autozygome filtration to identify homozygous mutations in coding sequences within the ROHs previously detected by SNP-microarray analysis. Screening for *WDR73* mutations in additional affected individuals and segregation validation were performed by Sanger sequencing. PCR primers (Table S1, available online) were designed with the program Primer3 according to RefSeq accession number NM_032856.2.

Plasmids, Cell Culture, and Establishment of Lentiviral Cell Lines

The lentiviral vector pLenti-GIII-CMV-HA, which contains the human *WDR73* coding sequence (GenBank clone accession number BC063392), was purchased from Applied Biological Materials. Two hemagglutinin (HA) tags were added to the WDR73 N terminus with the QuickChange site-directed mutagenesis kit according to the manufacturer's (Stratagene's) protocol. This construct, used for rescuing the WDR73-depleted podocyte phenotype, is called wild-type (WT) later in the text. Constructs were verified by Sanger sequencing. Lentiviral particles containing this construct were

produced by the lentivector production facility Structure Fédérative de Recherche BioSciences Gerland-Lyon Sud (UMS3444/US8). Two small hairpin RNAs (shRNAs) targeting the 3′ UTR of the human *WDR73* mRNA (clone IDs TRCN0000135232 and TRCN0000135695 from the RNAi Consortium) in the lentiviral vector pLKO.1 were purchased from Thermo Scientific. Lentiviral particles were produced in human embryonic kidney 293T cells as previously described.[10] Stably *WDR73*-depleted human podocyte cell lines were obtained by transduction with both types of shWDR73 lentiviral particles and subsequent puromycin selection (2 μg/ml).

Primary skin fibroblasts, herein called A-II-4 fibroblasts, were obtained from individual II-4 from family A (Figure 1A) and were subsequently grown in OPTIMEM medium supplemented with 10% fetal bovine serum, sodium pyruvate, glutamine, fungizone, and penicillin and streptomycin (all from Life Technologies) at 37°C with 7% CO_2.

A conditionally immortalized human podocyte cell line, developed by transfection with the temperature-sensitive mutant (tsA58) of the SV40-T-antigen-encoding gene, was kindly provided by M.A. Saleem (University of Bristol, Southmead Hospital, Bristol). In brief, the cells proliferated at the permissive temperature of 33°C, whereas growth arrest and differentiation were induced by incubation at the nonpermissive temperature of 37°C for 14 days. Cells were grown with 7% CO_2 in RPMI 1640 medium supplemented with 10% fetal bovine serum, insulin-transferrin-selenium, glutamine, and penicillin and streptomycin (all from Life Technologies).

Antibodies and Immunoblotting

Antibodies used for immunoblotting and immunofluorescence were mouse anti-GAPDH (Millipore), anti-HA (Covance), anti-α-tubulin (Sigma-Aldrich), rabbit anti-WDR73 (Sigma-Aldrich), goat anti-synaptopodin, anti-lamin B, and anti-γ tubulin (Santa Cruz), and Alexa Fluor-conjugated annexin V (Life Technologies).

Total cell lysate was extracted with lysis buffer (50 mM Tris-HCl, 150 mM NaCl, 0.5% sodium deoxycholate, 2 mM EDTA, 1% Triton X-100, and 0.1% SDS). A total of 100 μg of protein was loaded onto a 4%–20% acrylamide gel (Biorad) or a 12% gel, and immunoblotting was carried out with the indicated antibodies as previously described.[11]

Immunochemistry and Immunofluorescence

Five-micron-thick sections of formalin-fixed paraffin-embedded samples of human infant brain (3 months old) and fetal kidney (25 weeks of gestation) were obtained. Slides were dewaxed either in toluene or in Bioclear solution (Bio-Optica) for brain or kidney sections, respectively, and then immersed in water. Samples were boiled for 25 min in a water bath in antigen-retrieval solution (DakoCytomation) and subsequently cooled in the same solution at room temperature. Endogenous peroxidase activity was quenched by treatment in 0.3% H_2O_2 for 30 min. The sections were preincubated in normal serum diluted in PBS (10%) for 30 min for the prevention of nonspecific binding. The samples were then incubated with the anti-WDR73 primary antibody overnight at 4°C. The bound antibodies were visualized with an avidin-biotin peroxidase kit (VECTASTAIN, Vector Laboratories), and 3.3′-diaminobenzidine tetrahydrochloride (DAB) was used as a chromogen (DAB Peroxidase Substrate Kit, Vector Laboratories). Sections were counterstained with Mayer's hematoxylin, mounted, and observed with a Nikon optic microscope.

Fibroblasts and podocytes were plated on Lab-Tek Chamber Slides and on coverslips coated with rat-tail collagen type I (Corning), respectively. After 48 hr of culture, cells were fixed in either cold 100% methanol or 4% paraformaldehyde (PFA). PFA-fixed cells were treated with 50 mM NH_4Cl. Cells were incubated with a blocking solution (PBS, 1% BSA, and 0.1% tween 20) for 1 hr prior to primary antibody hybridization. For tissue sections, slides were treated as described above before antibody incubation. Cells and tissues were then probed with appropriate Alexa Fluor-conjugated secondary antibodies (Life Technologies), and nuclei were stained with Hoechst (Life Technologies).

For assessment of microtubule repolymerization, human podocytes were incubated with 30 μM of nocodazole (Sigma) for 4 hr at 33°C or 37°C for undifferentiated or differentiated podocytes, respectively. Cells were then washed with PBS, incubated at 33°C or 37°C, and fixed after 0, 5, or 60 min. Finally, immunofluorescence was carried out as described above.

For the annexin V (Life Technologies) assay, cells were first incubated with annexin V in 10 mM HEPES, 140 mM NaCl, and 25 mM $CaCl_2$ before PFA fixation, and then nuclei were stained with Hoechst. Confocal images were obtained with a Leica TCS-SP8 microscope, and posttreatment analysis was performed with Image J.

Cell-Proliferation Assay

Fibroblasts were seeded into 96-well plates at 8,000 cells per well in triplicate and were allowed to attach for 24 hr. Cell proliferation was assessed with the CellTiter 96 Aqueous Non-Radioactive Cell Proliferation Assay (MTT) (Promega) according to the manufacturer's protocol after 24, 48, 72, 96, and 120 hr of culture.

WDR73 Modeling

The structure of WDR73 was predicted with the WD40-Repeat Protein Structure Predictor (WDSP) [12,13] on the basis of WDR73 sequence from GenBank accession number AAF28942.1 (residues 73–370). The structure was manually inspected, and figures were drawn in MacPyMOL (Schrödinger).

Statistical Analysis

Results are presented as means ± SEM or SD. Statistical analysis was performed with the Student's t test for pairwise comparisons and the ANOVA test for comparisons involving three or more groups. Analysis was carried out with GraphPad Prism. A p value of <0.05 was considered statistically significant ($^*p < 0.05$; $^{**}p < 0.01$, $^{***}p < 0.005$). All experiments were performed at least three times.

Results

WDR73 Mutations in GMS

We performed autozygosity mapping combined with WES in a Moroccan family (family A) with two affected children to investigate the genetic basis of GMS. Both children developed secondary microcephaly and severe neurological impairment, and one also developed nephrotic syndrome (individual II-3 in family A; Figure 1A; Table 1). Genome-wide analysis with SNP arrays revealed that the affected siblings from family A share only one common ROH, which is 4.3 Mb in length and located on chromosome 15. This region contains 24 genes, one of which is

Table 1. Clinical and Pathological Phenotypes of Affected Individuals

	Family A		Family B
	II-3	II-4	II-3
Sex	male	male	male
Age of onset of proteinuria	NS at 5 years	no proteinuria	6 g/g at 8 years, 0.7 g/g at 13 years
Renal lesions	collapsing FSGS, podocyte hypertrophy	no (at 7 years)	FSGS, podocyte hypertrophy
Age of ESKD	5 years	no (at 7 years)	no (at 13 years)
Neurological features	secondary microcephaly (−1 SD at birth, −3 SDs at 5 years), peripheral hypertonia, axial hypotonia (diagnosed at 4 months), nystagmus, epileptic spasms, ID	secondary microcephaly (+1 SD at birth, −2.5 SDs at 2 years), peripheral and axial hypotonia (diagnosed at 4 months), epileptic spasms, ID	head circumference at −2 SDs at 5 months[a] and −3 SDs at 10 years, hypertonia, ID, spasticity
Brain MRI anomalies	cerebellar atrophy, thin corpus callosum	cerebellar atrophy, subtentorial atrophy	cerebellar atrophy, thin corpus callosum, subtentorial atrophy, ventricular dilation
Other features	facial dysmorphy, abnormal visual evoked potentials, optic atrophy, death at 5 years	facial dysmorphy, optic atrophy	facial dysmorphy, abnormal visual evoked potentials, optic atrophy

Abbreviations are as follows: ESKD, end-stage kidney disease; FSGS, focal segmental glomerulosclerosis; and ID, intellectual disability.
[a]No cranial circumference available at birth.

referenced in OMIM (*ZNF592* [MIM 613624]). Given the number of coding sequences in this ROH, we performed WES in one affected child (individual II-3 from family A). The average read coverage of chromosome 15 was 64×, and 77% of targeted bases were covered at least by 25 reads. A nonsense *WDR73* mutation (c.129T>G [p.Tyr43*]; RefSeq NM_032856.2) was the only homozygous damaging variant within the ROH (Figure S1). Next, we screened *WDR73* mutations in a cohort of 30 unrelated individuals with microcephaly and neurological impairment associated with glomerular lesions or isolated proteinuria. In one child from a consanguineous Turkish family, we detected another homozygous frameshift mutation in *WDR73* (c.766dupC [p.Arg256Profs*18]). Both mutations segregated with the disease (Figure 1A), and neither is referenced in the NHLBI Exome Variant Server or in dbSNP. In addition, we screened for mutations in *WDR73* in a group of 26 individuals with microcephaly but without obvious renal involvement or any mutation in known primary microcephaly-associated genes; however, we found no mutations.

WDR73 is predicted to encode a protein containing six WD40 motifs, which have an average score of 66.34 and an estimated accuracy of 89.5% in WDSP[12,13] (Figures 1B and 1C). The p.Tyr43* alteration truncates the protein precociously and is located upstream of all of the WD40 repeats, whereas the p.Arg256Profs*18 mutant is expected to contain four WD40 repeats (Figure 1B).

Phenotype of Individuals Carrying homozygous *WDR73* Mutations

All three affected children presented with a similar neurological phenotype consisting of severe intellectual disability and secondary microcephaly diagnosed at 4 or 5 months of age (Table 1). Two of the children also suffered from epilepsy. In all affected individuals, brain MRI showed major cerebellar atrophy without brainstem anomalies, a thin corpus callosum, moderate sustentorial atrophy, and mild ventricular dilation. No apparent myelin or gyration defects were observed (Figure 2A; Table 1). Affected individuals II-3 from family A and II-3 from family B (Figure 1A) developed NS, which was detected at 5 and 8 years of age, respectively. Individual II-3 from family A presented with steroid resistant NS at 5 years of age, rapidly developed chronic renal insufficiency, and eventually died within a month. Individual II-3 in family B had normal renal function at the last examination at 13 years of age. Kidney biopsies were performed in both of these children. In individual II-3 in family A, tissue sections revealed severe collapsing FSGS, characterized by the diffuse retraction of the glomerular tufts surrounded by hypertrophic podocytes and the focal development of segmental sclerotic lesions. Foci of interstitial fibrosis and tubular dilations were associated with glomerular lesions (Figure 2B; Table 1). Lesions were less severe in individual II-3 in family B (Figure 1A), which is consistent with normal renal function in this child. However, glomerular tufts were lined by hypertrophic and focally vacuolated podocytes, and FSGS lesions affecting a small percentage of glomeruli were present along with moderate tubulointerstitial lesions (Figure 2B; Table 1). Individual II-4 from family A (Figure 1A) had no proteinuria and had normal renal function at the last follow-up examination at the age of 7 years.

WDR73 Localization in the Human Kidneys and Brain

According to GeneCards, *WDR73* RNA is ubiquitously expressed in normal human tissues, including the brain and kidneys. We first sought to determine precisely the

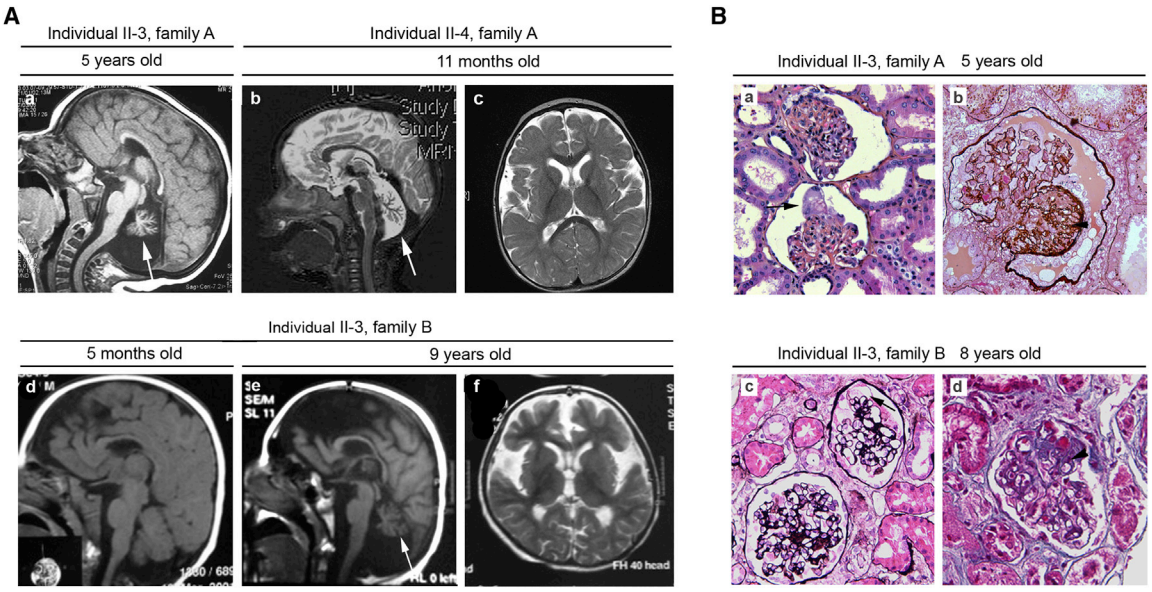

Figure 2. Neuroimaging and Renal Pathological Analysis
(A) MRI features of three affected individuals with GMS. Sagittal T1 (a, d, and e) and T2 (b) images are shown. Microcephaly with no gyration defect, a thin corpus callosum, and cortical and cerebellar (arrows) atrophy without brainstem anomalies were common in all affected individuals. Axial T2 images (c and f) are shown. Ventricular dilations with moderate subtentorial atrophy were observed in individuals II-4 in family A and II-3 in family B.
(B) Kidney sections of individuals with *WDR73* mutations. Individual II-3 in family A showed (a) a marked collapse of the glomerular tufts associated with podocyte hypertrophy (arrow; trichrome-safranin stain; 63× magnification) and (b) the presence of a FSGS lesion surrounded by a layer of enlarged podocytes. The adjacent capillary loops are retracted, and the capillary lumen is small (arrowhead; methenamine-silver stain; 100× magnification). Individual II-3 from family B showed (c) diffuse podocyte hypertrophy and periglomerular fibrosis and large vacuoles in some cells (arrow; methenamine-silver stain; 63× magnification) and (d) the presence of an FSGS lesion (arrowhead; trichrome-safranin stain in light green; 100× magnification).

localization of WDR73 in human fetal kidney and infant brain by performing immunochemistry staining on tissue sections. In fetal kidney, where all stages of nephrogenesis are present, we observed strong staining in immature podocytes from the S-shaped-body stage to the capillary-loop stage (Figure 3A, left and middle panels). In contrast to the persistent strong staining of the podocyte foot-process marker synaptopodin, WDR73 labeling was weaker at the late stages than at the early stages of glomerular maturation. In mature glomeruli, WDR73 had a punctuated distribution at the periphery of the glomerular tuft, outside the linear labeling of synaptopodin. This dissociated distribution suggests that WDR73 is present in the cell body of mature podocytes (Figure 3A, right panel). We also detected an intense punctuated WDR73 labeling in mature tubules (Figure 3A, right panel). In human infant brain, WDR73 was found in a large variety of cells. In the cerebellum, WDR73 immunostaining was strong in Purkinje cells and their projecting axons (Figure 3B, left panel), in the deep cerebellar nuclei (data not shown), and in pyramidal neurons of the cerebral cortex (Figure 3B, middle panel). In the white matter, WDR73 appeared to be mainly present in astrocytes, but not in oligodendrocytes (Figure 3B, right panel). Finally, endothelial cells of cerebral capillaries also displayed a high amount of WDR73 (Figure 3B, right panel). We observed a similar localization pattern in adult brain (data not shown).

WDR73 Subcellular Localization throughout the Cell Cycle and Its Role in Cell Viability

In control fibroblasts, WDR73 displayed weak and diffuse staining within the cytoplasm during interphase, whereas during mitosis, it strongly accumulated at the spindle poles and microtubule asters and later in the cleavage furrow (Figure 4). We observed a similar pattern in a human immortalized podocyte cell line that is commonly used as a cellular model for studying glomerulopathy[14] (Figure S2).

We sought to elucidate the function of WDR73; therefore, we characterized the cellular phenotype of fibroblasts from individual II-4 in family A and podocytes stably expressing shRNA against WDR73. In both cell lines, the abundance of WDR73 was drastically lower than that in the control cell lines (Figure S3A).

Interestingly, in A-II-4 fibroblasts, we observed striking abnormalities in the size and shape of the nuclei, such as budding or flecking nuclei or multinucleated cells (Figure 5A). Given that these nuclear abnormalities strongly suggest a defect in cell viability,[15] we conducted a cell-proliferation assay and found that cell survival was lower in A-II-4 fibroblasts than in control cells (Figure 5B). This difference could have been due to either a defect in cell proliferation or a higher rate of apoptosis. Annexin V labeling showed that the rate of apoptosis was higher in A-II-4 fibroblasts than in control cells

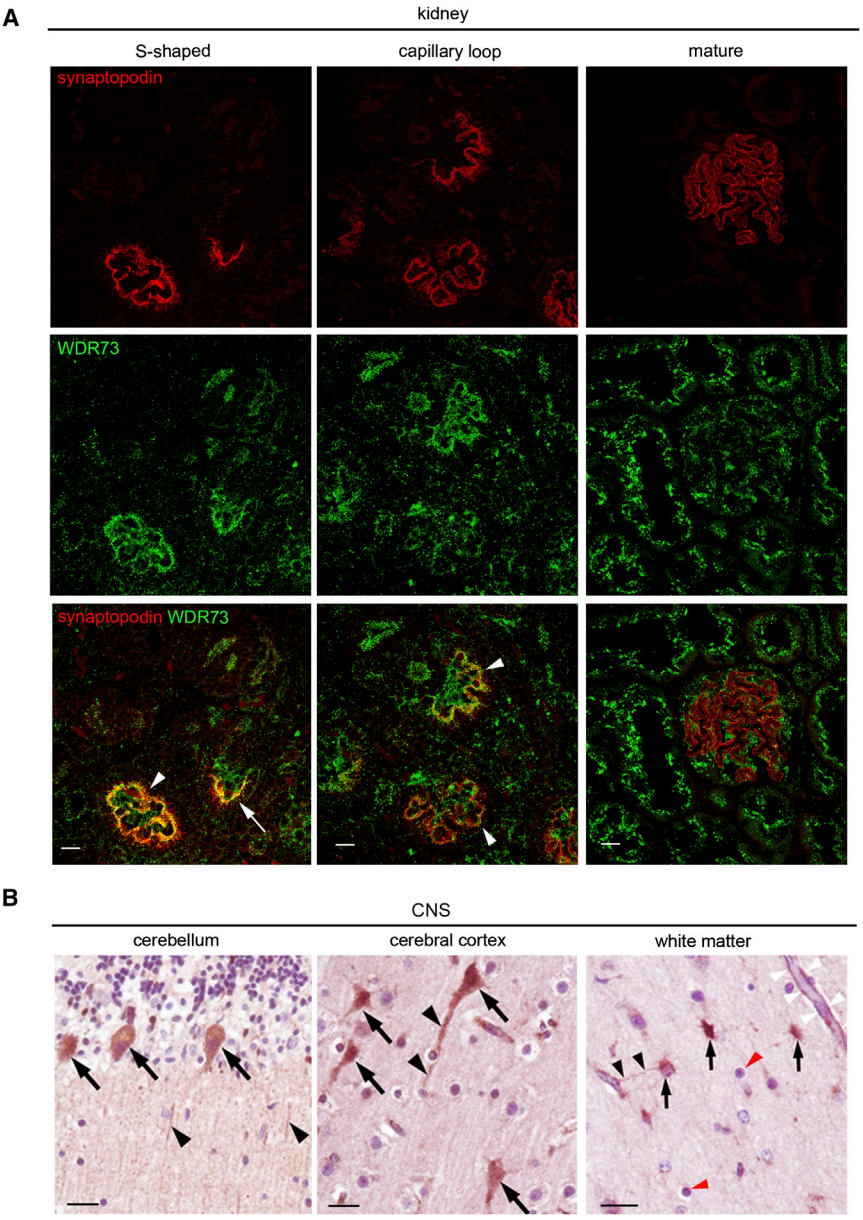

Figure 3. WDR73 Localization in Kidneys and Brain

(A) Immunofluorescence in normal human kidney sections shows the localization of WDR73 (in green) and synaptopodin (in red). During kidney development, strong labeling of WDR73 was observed from the S-shaped-body stage (white arrow) to the capillary-loop stage (arrowhead) and decreased along glomerulus maturation.

(B) Immunoperoxidase staining of endogenous WDR73 in the infant CNS. WDR73 localized to the cell body of Purkinje cells in the cerebellum (left panel, arrows), in pyramidal neurons in the cerebral cortex (middle panel, arrows), and in their projecting axons (left and middle panels, arrowheads). In the white matter (right panel), WDR73 antibodies stained the cell body of astrocytes (arrows) and their cell processes (black arrowheads) and also endothelial cells of cerebral capillaries (white arrowheads). WDR73 was not detected in oligodendrocytes (red arrowheads).

Scale bars represent 20 μm.

(Figure 5C). WDR73-depleted podocytes also presented nuclear abnormalities, mainly multilobulated nuclei. This phenotype was rescued by reintroduction of the wild-type protein (Figure 5A). However, no cell-survival defect was observed, which could have been due to the immortalization of podocytes (Figure S3B).

Role of WDR73 in Organization of the Microtubule Network

Gerlitz et al.[16] showed that newly synthesized microtubules anchored at the centriole generate pressure in the nucleus and thus transiently disturb its shape in physiological conditions. Once the microtubule network is reorganized, the nucleus returns to its usual shape. We thus wondered whether dysregulation of the microtubule network could be responsible for the abnormal nuclear shape in WDR73-depleted podocytes (Figure 6, upper panel). We treated undifferentiated podocytes with nocodazole to depolymerize microtubules and monitored microtubule growth and nuclear morphology. After complete depolymerization, nuclear shape was restored, and cytosolic tubulin aggregates appeared in WDR73-depleted podocytes (Figure 6, middle panel). After 1 hr of repolymerization, the ratio of abnormally shaped nuclei to normal nuclei was higher in WDR73-depleted cells than in control cells (Figure 6, lower panel). In addition, WDR73-depleted cells displayed dense and disorganized microtubule aggregates around the nucleus, whereas control cells showed well-spread and -distributed microtubule cables (Figure 6, lower panel).

We and others have shown that differentiated podocytes are delicate cells, and the maintenance of their architecture requires fine regulation of microtubule and actin dynamics.[17–19] Therefore, we also studied the organization of the microtubule network in differentiated WDR73-depleted podocytes. Whereas control and wild-type-re-expressing cells were spread with a partial localization of WDR73 adjacent to microtubule cables, the depleted cells clearly showed a loss of WDR73 along the microtubules and presented an abnormal shape (Figure 7A), also found in A-II-4 fibroblasts (Figure S4A). Similar to that in control cells, the presence of synaptopodin in differentiated WDR73-depleted podocytes suggests that WDR73

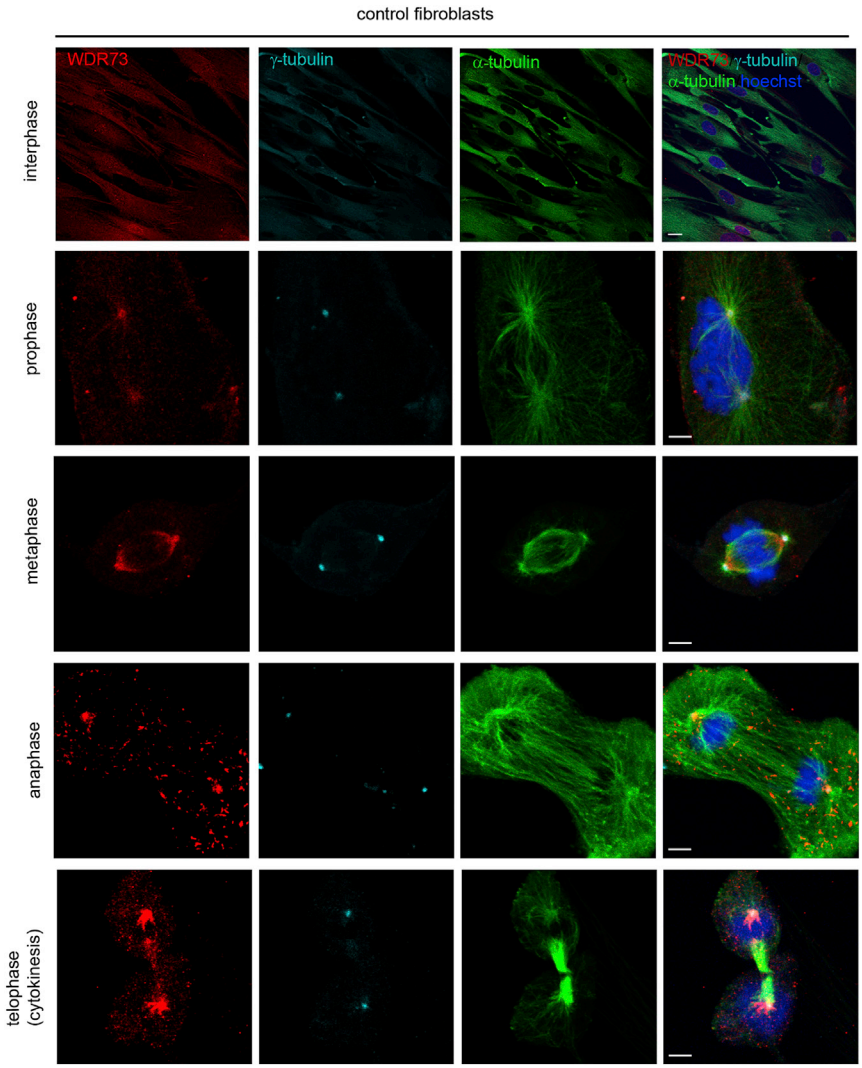

Figure 4. WDR73 Localization during the Cell Cycle

Immunolabeling of WDR73 (in red), γ-tubulin (in cyan), a marker of the centrioles, and α-tubulin (in green) in control fibroblasts. During interphase, a weak cytosolic staining of WDR73 was observed. However, during mitosis (from prophase to anaphase), WDR73 relocalized to microtubule asters and the cleavage furrow. Scale bars represent 10 μm.

deficiency does not impair podocyte differentiation (Figure S4B). We then treated differentiated podocytes with nocodazole as described above and examined the polymerization of microtubules into the aster after 5 min of recovery. The diameter of the asters was smaller in WDR73-depleted podocytes than in control cells (Figure 7B, left and middle panels). This alteration, which is a hallmark of a delay in microtubule polymerization,[20] was rescued by re-expression of the wild-type construct (Figure 7B, right panel). Altogether, these data suggest a crucial role for WDR73 in the regulation of microtubule dynamics and organization during interphase.

Discussion

Through autozygosity mapping, WES, and subsequent genotyping in a small cohort of individuals with GMS, we identified two truncating homozygous mutations in *WDR73* in two families. The detection of mutations in a small subset of GMS-affected individuals (2 out of 31) further substantiates the idea that GMS is a genetically heterogeneous disease (an idea that was already suspected from its clinical heterogeneity). The main clinical manifestations in these two families were postnatal microcephaly diagnosed within the first year of life, marked cerebellar atrophy, severe intellectual disability, and late-onset NS. However, an important interfamilial and intrafamilial variability was observed for the severity of the renal phenotype: one affected child (individual II-4 in family A) showed no symptoms at the age of 7 years. This is reminiscent of what was observed in some families affected by early-onset NS and mutations in *PLCE1* (MIM 608414).[21–23] Furthermore, no additional mutations in genes known to be mutated in hereditary NS were found in these affected individuals, which could not explain the clinical heterogeneity of the renal phenotype. Conversely, we tested *WDR73* in 26 individuals with microcephaly without renal involvement and did not find any mutation, suggesting that *WDR73* is not involved in isolated microcephaly. Nevertheless, we suggest that physicians should screen for proteinuria in children with a neurological phenotype similar to that described above. Altogether, our data show that mutations in *WDR73* cause GMS.

WDR73 encodes a protein containing WD40 repeats, which are motifs of approximately 40–60 amino acid residues usually ending with Trp-Asp (WD).[24] Each WD40 repeat folds into a four-stranded antiparallel β sheet blade. These blades often assemble into domains containing a seven-bladed propeller called the WD40 domain. These domains act as platforms for protein assembly, making them hubs in many cell-signaling networks.[24] Several genes encoding WD40-domain proteins have already been implicated in human genetic disorders.[25–27] WDR73 is predicted to harbor six WD40 repeats leading to an incomplete six-bladed propeller protein. Some proteins, such as Seh1 and Sec, only have a six-bladed propeller, which interacts with another blade from a donor protein—Nup85 and Nup145, respectively—to form a β propeller with seven

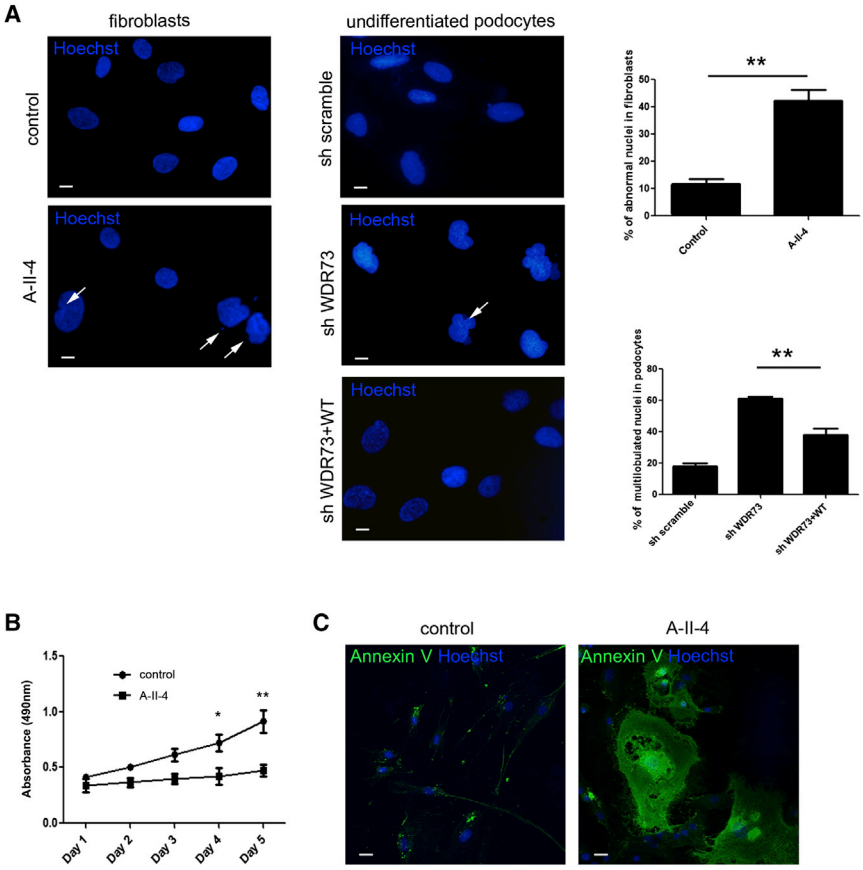

Figure 5. Phenotype of WDR73-Depleted Podocytes and Fibroblasts

(A) Hoechst staining in fibroblasts (left panel) and podocytes (right panel). A-II-4 fibroblasts and WDR73-depleted podocytes displayed alterations in nuclear morphology, including budding, multilobulation (white arrows), shrinkage, or fragmentation. For generating the graphical quantification of the number of nuclear alterations, 100 nuclei from ten random fields in each condition were observed and classified as having either a normal or an abnormal nuclear shape. The Student's t test was used for comparing differences between A-II-4 and control fibroblasts. The mean ± SEM is shown (* $p < 0.05$; ** $p < 0.01$). Scale bars represent 20 μm.

(B) Graph showing the results of the colorimetric cell-proliferation assay (MTT) in fibroblasts. The viability of A-II-4 cells was significantly lower than that of control cells. The Student's t test was used for comparing differences between A-II-4 and control fibroblasts. The mean ± SEM is shown (* $p < 0.05$; ** $p < 0.01$).

(C) Immunolabeling of annexin V shows a higher rate of apoptosis in A-II-4 fibroblasts than in control fibroblasts. Scale bars represent 10 μm.

blades.[28] We can therefore hypothesize that WDR73 requires the association of another partner to form a complete standard propeller. *WDR73* mutations, leading to the deletion of WD40 repeats, might prevent the assembly of this β propeller structure, thus impairing the recruitment of its partners.

Our experiments in various cell models clearly suggest a role for WDR73 in cell survival and microtubule regulation. We have shown that WDR73 is localized in the cytoplasm during interphase and then accumulates at the spindle poles and microtubule asters during mitosis. This behavior resembles that of proteins encoded by genes mutated in primary microcephaly, namely *CENPJ* (MIM 609279),[29] *ASPM* (MIM 605481),[30,31] and *WDR62* (MIM 613583).[25,27,32] Therefore, it is tempting to speculate that WDR73, similar to WDR62, is involved in mitosis in neural precursors during embryonic life. However, the head circumference of individuals at birth appeared normal, suggesting that the proliferation of neuronal precursors was normal; instead, we hypothesize that WDR73 has an important role in neuronal cell survival. Indeed, the cerebellar atrophy and the secondary microcephaly observed in these children could be due to a high rate of cells entering apoptosis, as observed in A-II-4 fibroblasts. In addition, the microtubule-polymerization defects observed in the cell lines and the localization of WDR73 in a large variety of neurons and their projecting axons in both the cerebral and cerebellar cortex suggest that WDR73 is also involved in the organization of neuronal and axonal microtubule networks.[33] Indeed, fine regulation of the microtubule network is crucial for the completion of brain development and is required for dendritic and axonal arborization and growth, myelination, and synaptogenesis during the first years of life in both the cerebellum and the brain cortex.[34]

Our findings in the kidney support the idea that WDR73 plays a role in the regulation of the microtubule network, which is consistent with recent data on hereditary NS and FSGS. Indeed, genetic studies have identified >20 NS- and FSGS-associated genes, which mainly encode proteins expressed in podocytes.[35] This highly differentiated cell has an octopus-like shape with microtubule-enriched primary processes and interdigitated actin-rich secondary foot processes bridged by the slit diaphragm. These genes mainly encode slit-diaphragm components and actin-cytoskeleton regulators that confer to the podocyte its precise shape and plasticity. Mutations in these genes result in foot-process effacement driven by the global reorganization of the actin cytoskeleton and subsequent protein leakage in the urine. More recently, the identification of mutations in genes encoding microtubule regulators, such as *INF2* (MIM 610982),[18] and *TTC21B* (MIM 612014),[19] also suggests that the integrity of the slit diaphragm depends on microtubules, which are crucial for the maintenance of cell architecture and protein trafficking. Interestingly, the distinct

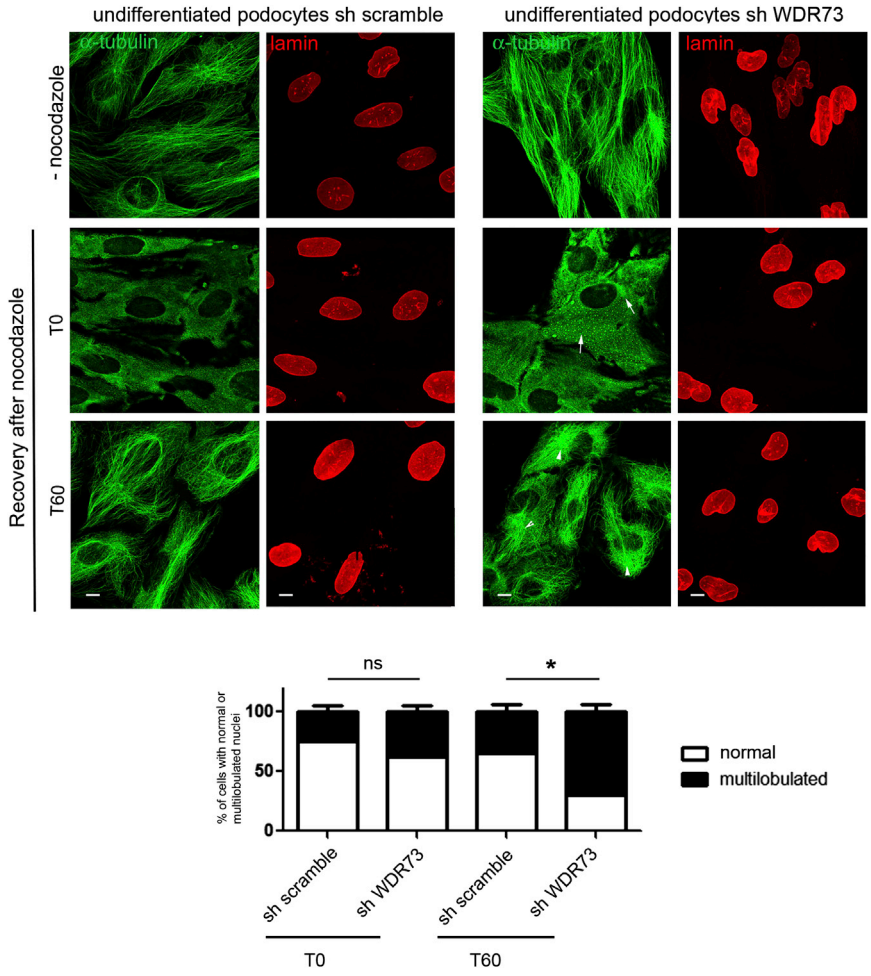

Figure 6. Effect of WDR73 Invalidation on Microtubule Polymerization and Nuclear Shape in Undifferentiated Podocytes

Immmunolabeling of α-tubulin (in green) and lamin (in red), a marker of the nuclear envelope, before and after nocodazole treatment. After microtubule depolymerization induced by 4 hr incubation with nocodazole (T0), the shape of the nucleus in WDR73-depleted cells became similar to that in control cells, and microtubule aggregates within the cytosol were observed (white arrows). After microtubule repolymerization (T60), WDR73-depleted cells contained a nonhomogenous repartition of microtubules cables (arrow head) that did not properly diffuse within the cytosol, and the nucleus became multilobulated. A graph at T0 and T60 shows the number of multilobulated cells during the microtubule-regrowth assay. The Student's t test was used for comparing differences between WDR73-depleted and control podocytes. The mean ± SEM is shown (ns, not significant; *$p < 0.05$; **$p < 0.01$). Scale bars represent 20 μm.

immunostaining patterns of WDR73 and the actin-associated protein synaptopodin suggest that WDR73 preferentially localizes to the microtubule-enriched primary foot processes and not to the actin-rich secondary foot processes.

Although podocytes and neurons are highly differentiated cells, which are very dissimilar in terms of structure and function, both cell types share many common biological features.[36–38] Neurons and podocytes are both organized into a main cell body, giving rise to multiple projections that subsequently form axons and dendrites in neurons and primary foot processes in podocytes with the same atypical microtubule polarity.[39] In addition, several structural and regulatory proteins—such as synaptopodin,[40] Huntingtin-interacting protein 1, neurofascin, and olfactomedin-like 2a[38]—are specifically localized in both neurons and podocytes. Other similarities between podocytes and neurons include the presence of functional-neuron-like synaptic vesicles in podocytes[41] and the importance of glutamatergic signaling, which in podocytes contributes to the integrity of the glomerular-filtration barrier.[42] However, there are still very few examples of genes in which mutations have been identified as responsible for genetic diseases impairing both the glomerulus and the nervous system. Mutations in *INF2* affect podocytes, Schwann cells, and peripheral nerve axons, leading to a disease associating an intermediate neuropathy with impaired glomerular function. *WDR73* is another example of a gene in which mutations result in this dual phenotype, providing additional evidence of the existence of common molecular processes of development and maintenance in the glomerulus and the nervous system.[36]

In conclusion, we have demonstrated that mutations in *WDR73* are responsible for GMS. The implication of WDR73 in the regulation of the microtubule network during the cell cycle suggests that it plays a crucial role in the development and maturation of the nervous system and in the maintenance of the proper function and integrity of glomerular filtration. The identification of proteins interacting with WDR73 and/or mutations in other genes associated with GMS will shed more light on the role of WDR73 and the pathophysiology of this very rare condition.

Supplemental Data

Supplemental Data include four figures and one table and can be found with this article online at http://dx.doi.org/10.1016/j.ajhg.2014.10.011.

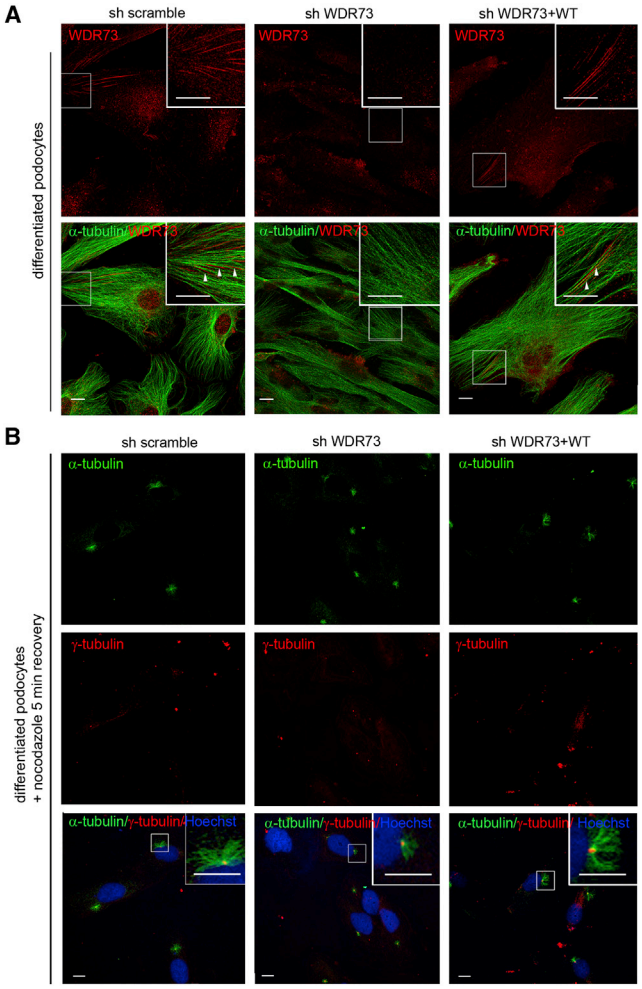

Figure 7. Effect of WDR73 Depletion on Microtubule Polymerization and Cell Shape in Differentiated Podocytes
(A) Immunostaining of WDR73 (in red) and α-tubulin (in green) in differentiated podocytes. WDR73 localized adjacent to some microtubule cables (arrow heads). WDR73 depletion was associated with abnormal morphology and altered WDR73 localization, which was rescued by the wild-type protein.
(B) Nocodazole treatment in differentiated podocytes was conducted before immunolabeling with γ-tubulin (in red) and α-tubulin (in green) antibodies. After 5 min of microtubule regrowth, WDR73-depleted podocytes displayed a delay in microtubule polymerization, which was restored by reintroduction of the wild-type protein.
Scale bars represent 20 μm.

Acknowledgments

We thank Moin A. Saleem for kindly providing the conditionally immortalized human podocyte cell line. We greatly acknowledge the Necker Institute cell-imaging facility for providing expert knowledge on confocal microscopy. We are grateful to Integragen for exome sequencing. We thank Gisèle Froment, Didier Nègre, and Caroline Costa from the lentivector production facility Structure Fédérative de Recherche Biosciences Gerland-Lyon Sud (UMS3444/US8). We thank all the individuals with Galloway-Mowat syndrome and their families for their participation in this study. We thank Kalman Tory and Sophie Saunier for helpful discussions. Financial support for this work was provided by grants from the Agence Nationale de la Recherche (GenPod project ANR-12-BSV1-0033.01), the European Union's Seventh Framework Programme (FP7/2007-2013/n°305608-EURenOmics), and the "Investments for the Future" program (ANR-10-IAHU-01) to C.A., from the Angers University Hospital to E.C., and from the Ministère de l'Education Nationale de la Recherche et de la Technologie to E.H.C.

Received: September 24, 2014
Accepted: October 24, 2014
Published: November 13, 2014

Web Resources

The URLs for data presented herein are as follows:

dbSNP, http://www.ncbi.nlm.nih.gov/SNP/
Ensembl, http://www.ensembl.org/index.html
GenBank, http://www.ncbi.nlm.nih.gov/genbank/
GeneCards, http://www.genecards.org/
The Human Protein Atlas, http://www.proteinatlas.org/
NHLBI Exome Sequencing Project (ESP) Exome Variant Server, http://evs.gs.washington.edu/EVS/
Online Mendelian Inheritance in Man (OMIM), http://www.omim.org/
Primer3, http://primer3.ut.ee/
RefSeq, http://www.ncbi.nlm.nih.gov/refseq/
WD40-Repeat Structure Predictor (WDSP), http://wu.scbb.pkusz.edu.cn/wdsp/

References

1. Pezzella, M., Yeghiazaryan, N.S., Veggiotti, P., Bettinelli, A., Giudizioso, G., Zara, F., Striano, P., and Minetti, C. (2010). Galloway-Mowat syndrome: an early-onset progressive encephalopathy with intractable epilepsy associated to renal impairment. Two novel cases and review of literature. Seizure *19*, 132–135.
2. Galloway, W.H., and Mowat, A.P. (1968). Congenital microcephaly with hiatus hernia and nephrotic syndrome in two sibs. J. Med. Genet. *5*, 319–321.
3. Ekstrand, J.J., Friedman, A.L., and Stafstrom, C.E. (2012). Galloway-Mowat syndrome: neurologic features in two sibling pairs. Pediatr. Neurol. *47*, 129–132.
4. Meyers, K.E., Kaplan, P., and Kaplan, B.S. (1999). Nephrotic syndrome, microcephaly, and developmental delay: three separate syndromes. Am. J. Med. Genet. *82*, 257–260.
5. Hazza, I., and Najada, A.H. (1999). Late-onset nephrotic syndrome in galloway-mowat syndrome: a case report. Saudi J. Kidney Dis. Transpl. *10*, 171–174.
6. Steiss, J.O., Gross, S., Neubauer, B.A., and Hahn, A. (2005). Late-onset nephrotic syndrome and severe cerebellar atrophy in Galloway-Mowat syndrome. Neuropediatrics *36*, 332–335.
7. Kang, L., Kuo, P.-L., Lee, K.-H., Liu, Y.-C., Chang, C.-H., Chang, F.-M., and Lin, S.-J. (2005). Late-onset growth restriction in Galloway-Mowat syndrome: a case report. Prenat. Diagn. *25*, 159–162.
8. Sartelet, H., Pietrement, C., Noel, L.-H., Sabouraud, P., Birembaut, P., Oligny, L.L., Roussel, B., and Doco-Fenzy, M. (2008). Collapsing glomerulopathy in Galloway-Mowat syndrome: a case report and review of the literature. Pathol. Res. Pract. *204*, 401–406.

9. Dietrich, A., Matejas, V., Bitzan, M., Hashmi, S., Kiraly-Borri, C., Lin, S.-P., Mildenberger, E., Hoppe, B., Palm, L., Shiihara, T., et al. (2008). Analysis of genes encoding laminin beta2 and related proteins in patients with Galloway-Mowat syndrome. Pediatr. Nephrol. *23*, 1779–1786.
10. Mahuzier, A., Gaudé, H.-M., Grampa, V., Anselme, I., Silbermann, F., Leroux-Berger, M., Delacour, D., Ezan, J., Montcouquiol, M., Saunier, S., et al. (2012). Dishevelled stabilization by the ciliopathy protein Rpgrip1l is essential for planar cell polarity. J. Cell Biol. *198*, 927–940.
11. Mollet, G., Ratelade, J., Boyer, O., Muda, A.O., Morisset, L., Lavin, T.A., Kitzis, D., Dallman, M.J., Bugeon, L., Hubner, N., et al. (2009). Podocin inactivation in mature kidneys causes focal segmental glomerulosclerosis and nephrotic syndrome. J. Am. Soc. Nephrol. *20*, 2181–2189.
12. Wu, X.-H., Wang, Y., Zhuo, Z., Jiang, F., and Wu, Y.-D. (2012). Identifying the hotspots on the top faces of WD40-repeat proteins from their primary sequences by β-bulges and DHSW tetrads. PLoS ONE *7*, e43005.
13. Wang, Y., Jiang, F., Zhuo, Z., Wu, X.-H., and Wu, Y.-D. (2013). A method for WD40 repeat detection and secondary structure prediction. PLoS ONE *8*, e65705.
14. Saleem, M.A., O'Hare, M.J., Reiser, J., Coward, R.J., Inward, C.D., Farren, T., Xing, C.Y., Ni, L., Mathieson, P.W., and Mundel, P. (2002). A conditionally immortalized human podocyte cell line demonstrating nephrin and podocin expression. J. Am. Soc. Nephrol. *13*, 630–638.
15. Yu, C.-S., Huang, A.-C., Lai, K.-C., Huang, Y.-P., Lin, M.-W., Yang, J.-S., and Chung, J.-G. (2012). Diallyl trisulfide induces apoptosis in human primary colorectal cancer cells. Oncol. Rep. *28*, 949–954.
16. Gerlitz, G., Reiner, O., and Bustin, M. (2013). Microtubule dynamics alter the interphase nucleus. Cell. Mol. Life Sci. *70*, 1255–1268.
17. Welsh, G.I., and Saleem, M.A. (2012). The podocyte cytoskeleton—key to a functioning glomerulus in health and disease. Nat. Rev. Nephrol. *8*, 14–21.
18. Boyer, O., Nevo, F., Plaisier, E., Funalot, B., Gribouval, O., Benoit, G., Huynh Cong, E., Arrondel, C., Tête, M.-J., Montjean, R., et al. (2011). INF2 mutations in Charcot-Marie-Tooth disease with glomerulopathy. N. Engl. J. Med. *365*, 2377–2388.
19. Huynh Cong, E., Bizet, A.A., Boyer, O., Woerner, S., Gribouval, O., Filhol, E., Arrondel, C., Thomas, S., Silbermann, F., Canaud, G., et al. (2014). A Homozygous Missense Mutation in the Ciliary Gene TTC21B Causes Familial FSGS. J. Am. Soc. Nephrol. Published online May 29, 2014. http://dx.doi.org/10.1681/ASN.2013101126.
20. Recino, A., Sherwood, V., Flaxman, A., Cooper, W.N., Latif, F., Ward, A., and Chalmers, A.D. (2010). Human RASSF7 regulates the microtubule cytoskeleton and is required for spindle formation, Aurora B activation and chromosomal congression during mitosis. Biochem. J. *430*, 207–213.
21. Gbadegesin, R., Hinkes, B.G., Hoskins, B.E., Vlangos, C.N., Heeringa, S.F., Liu, J., Loirat, C., Ozaltin, F., Hashmi, S., Ulmer, F., et al. (2008). Mutations in PLCE1 are a major cause of isolated diffuse mesangial sclerosis (IDMS). Nephrol. Dial. Transplant. *23*, 1291–1297.
22. Hinkes, B., Wiggins, R.C., Gbadegesin, R., Vlangos, C.N., Seelow, D., Nürnberg, G., Garg, P., Verma, R., Chaib, H., Hoskins, B.E., et al. (2006). Positional cloning uncovers mutations in PLCE1 responsible for a nephrotic syndrome variant that may be reversible. Nat. Genet. *38*, 1397–1405.
23. Gilbert, R.D., Turner, C.L.S., Gibson, J., Bass, P.S., Haq, M.R., Cross, E., Bunyan, D.J., Collins, A.R., Tapper, W.J., Needell, J.C., et al. (2009). Mutations in phospholipase C epsilon 1 are not sufficient to cause diffuse mesangial sclerosis. Kidney Int. *75*, 415–419.
24. Xu, C., and Min, J. (2011). Structure and function of WD40 domain proteins. Protein Cell *2*, 202–214.
25. Bilgüvar, K., Oztürk, A.K., Louvi, A., Kwan, K.Y., Choi, M., Tatli, B., Yalnizoğlu, D., Tüysüz, B., Cağlayan, A.O., Gökben, S., et al. (2010). Whole-exome sequencing identifies recessive WDR62 mutations in severe brain malformations. Nature *467*, 207–210.
26. Li, D., and Roberts, R. (2001). WD-repeat proteins: structure characteristics, biological function, and their involvement in human diseases. Cell. Mol. Life Sci. *58*, 2085–2097.
27. Yu, T.W., Mochida, G.H., Tischfield, D.J., Sgaier, S.K., Flores-Sarnat, L., Sergi, C.M., Topçu, M., McDonald, M.T., Barry, B.J., Felie, J.M., et al. (2010). Mutations in WDR62, encoding a centrosome-associated protein, cause microcephaly with simplified gyri and abnormal cortical architecture. Nat. Genet. *42*, 1015–1020.
28. Hsia, K.-C., Stavropoulos, P., Blobel, G., and Hoelz, A. (2007). Architecture of a coat for the nuclear pore membrane. Cell *131*, 1313–1326.
29. Bond, J., Roberts, E., Springell, K., Lizarraga, S.B., Scott, S., Higgins, J., Hampshire, D.J., Morrison, E.E., Leal, G.F., Silva, E.O., et al. (2005). A centrosomal mechanism involving CDK5RAP2 and CENPJ controls brain size. Nat. Genet. *37*, 353–355.
30. Bond, J., Roberts, E., Mochida, G.H., Hampshire, D.J., Scott, S., Askham, J.M., Springell, K., Mahadevan, M., Crow, Y.J., Markham, A.F., et al. (2002). ASPM is a major determinant of cerebral cortical size. Nat. Genet. *32*, 316–320.
31. Fish, J.L., Kosodo, Y., Enard, W., Pääbo, S., and Huttner, W.B. (2006). Aspm specifically maintains symmetric proliferative divisions of neuroepithelial cells. Proc. Natl. Acad. Sci. USA *103*, 10438–10443.
32. Nicholas, A.K., Khurshid, M., Désir, J., Carvalho, O.P., Cox, J.J., Thornton, G., Kausar, R., Ansar, M., Ahmad, W., Verloes, A., et al. (2010). WDR62 is associated with the spindle pole and is mutated in human microcephaly. Nat. Genet. *42*, 1010–1014.
33. Lewis, T.L., Jr., Courchet, J., and Polleux, F. (2013). Cell biology in neuroscience: Cellular and molecular mechanisms underlying axon formation, growth, and branching. J. Cell Biol. *202*, 837–848.
34. Friede, R.L. (1973). Dating the development of human cerebellum. Acta Neuropathol. *23*, 48–58.
35. Akchurin, O., and Reidy, K.J. (2014). Genetic causes of proteinuria and nephrotic syndrome: Impact on podocyte pathobiology. Pediatr. Nephrol. Published online March 2, 2014. http://dx.doi.org/10.1007/s00467-014-2753-3.
36. Kobayashi, N., Gao, S.Y., Chen, J., Saito, K., Miyawaki, K., Li, C.Y., Pan, L., Saito, S., Terashita, T., and Matsuda, S. (2004). Process formation of the renal glomerular podocyte: is there common molecular machinery for processes of podocytes and neurons? Anat. Sci. Int. *79*, 1–10.
37. Sun, Y., Zhang, H., Hu, R., Sun, J., Mao, X., Zhao, Z., Chen, Q., and Zhang, Z. (2014). The expression and significance of neuronal iconic proteins in podocytes. PLoS ONE *9*, e93999.

38. Sistani, L., Rodriguez, P.Q., Hultenby, K., Uhlen, M., Betsholtz, C., Jalanko, H., Tryggvason, K., Wernerson, A., and Patrakka, J. (2013). Neuronal proteins are novel components of podocyte major processes and their expression in glomerular crescents supports their role in crescent formation. Kidney Int. *83*, 63–71.
39. Kobayashi, N., Reiser, J., Kriz, W., Kuriyama, R., and Mundel, P. (1998). Nonuniform microtubular polarity established by CHO1/MKLP1 motor protein is necessary for process formation of podocytes. J. Cell Biol. *143*, 1961–1970.
40. Mundel, P., Heid, H.W., Mundel, T.M., Krüger, M., Reiser, J., and Kriz, W. (1997). Synaptopodin: an actin-associated protein in telencephalic dendrites and renal podocytes. J. Cell Biol. *139*, 193–204.
41. Rastaldi, M.P., Armelloni, S., Berra, S., Calvaresi, N., Corbelli, A., Giardino, L.A., Li, M., Wang, G.Q., Fornasieri, A., Villa, A., et al. (2006). Glomerular podocytes contain neuron-like functional synaptic vesicles. FASEB J. *20*, 976–978.
42. Giardino, L., Armelloni, S., Corbelli, A., Mattinzoli, D., Zennaro, C., Guerrot, D., Tourrel, F., Ikehata, M., Li, M., Berra, S., et al. (2009). Podocyte glutamatergic signaling contributes to the function of the glomerular filtration barrier. J. Am. Soc. Nephrol. *20*, 1929–1940.